

HiSST: 4th International Conference on High-Speed Vehicle Science Technology 22 -26 September 2025, Tours, France



Fabrication of Reaction Bonded Silicon Carbide Components for Morphing Control Surfaces via Laser Powder Bed Fusion (LPBF) 3D-Printing: Challenges and Future Perspectives

Sebastian Meyers¹, Waut Declercq¹, Jef Vleugels², Brecht Van Hooreweder¹, Sébastien Paris³, Stéphane Débaisieux⁴, Manon Wouters⁴, Arnaud François⁵, Erin Kuçi⁵, Antoine Parmentier⁵, Johan Steelant⁶

Abstract

This paper addresses the processing of morphing structures for moving control surfaces in re-entry vehicles. To this end, laser powder bed fusion (LPBF) additive manufacturing (AM) was used to fabricate reaction bonded silicon carbide (RBSC) components. The production process consisted of powder preparation, LPBF, polymer infiltration and pyrolysis (PIP), SiC conversion, secondary PIP and liquid silicon infiltration (LSI) resulting in a fully dense RBSC. Components were produced for microstructural, mechanical, and thermal analysis. Results of these analyses were used as input for the design of a number of components with geometries more representative for the final application, i.e. morphable flaps for re-entry vehicles. These designs were subsequently fabricated and tested in a high-enthalpy flow in a Plasmatron facility. Although fabrication of these large samples was very challenging, two different designs were successfully fabricated and tested. During testing, failure occurred due to a sudden temperature increase in the Plasmatron facility. However, one test was successfully completed, showing limited morphing capability of the component. A total deflection of about 2 mm over a length of 90 mm was achieved, which corresponds to a bending radius of approximately 2 m. Future research should focus on creating a more morphable material, perhaps by making use of multi-material AM. In addition, challenges were identified during the printing of large components which need to be addressed.

Keywords: Thermal Protection Systems, Silicon Carbide, 3D-Printing, Morphing

Nomenclature

Symbols

d₅₀ – Median particle size, μm

E – Young's modulus, GPa

 ϵ – Elongation at break, %

h – Hatch spacing, µm

k – Thermal conductivity, W/mK

I – Layer thickness, µm

m – Weibull Modulus, -

v – Poisson coefficient, -

P - Laser power, W

ρ – Specific weight, g/cm³

 σ_{char} – Characteristic flexural strength, MPa

 σ_{flex} – Flexural strength, MPa

T – Temperature, °C

t - Time, h

v – Scanning speed, mm/s

HiSST-2025-#241 Page | 1

¹ KU Leuven, Department of Mechanical Engineering, Celestijnenlaan 300, 3001 Leuven, Belgium, sebastian.meyers@kuleuven.be

² KU Leuven, Department of Materials Engineering, Kasteelpark 44, 3001 Leuven, Belgium

³ Von Karman Institute, St. Genesius Rode, Belgium

⁴ Sonaca, Charleroi, Belgium

⁵ Cenaero, Charleroi, Belgium

⁶ ESA ESTEC, Noordwijk, The Netherlands

Abbreviations

AM – Additive Manufacturing

CTE – Coefficient of Thermal Expansion

IET – Impulse Excitation Technique

LPBF – Laser Powder Bed Fusion

LSI – Liquid Silicon Infiltration

PIP – Polymer Infiltration & Pyrolysis PM – Powder Metallurgy RBSC – Reaction Bonded Silicon Carbide TPS – Thermal Protection Systems

1. Introduction

Moveable control surfaces play an important role in the flight characteristics of aerospace vehicles. When considering Thermal Protection Systems (TPS) for these control surfaces, care should be taken to ensure appropriate design and integration with the rest of the vehicle. Specifically for moveable control surfaces, like flaps or slats, suitable sealing should be present to prevent dangerous leak flows towards the inner "cold" structure of the vehicle. In addition, the introduction of weak points due to surface discontinuities in the aggressive high-enthalpy environment should be avoided at all costs. To this end, hypersonic morphing could offer potential benefits by providing functionality in a continuous shape. However, research into hypersonic morphing is still in its infancy, and therefore, hypersonic morphing is still in an early, conceptual stage. The work done in this study aims to make advancements in the field of hypersonic morphing by combining smart design, simulations, and advanced production techniques for high-temperature materials. This paper specifically focuses on material and production techniques for morphable control surfaces.

Silicon carbide ceramics are lightweight and provide high temperature resistance and chemical stability, making them interesting candidate materials for hot structures. Indeed, SiC ceramics are frequently used as TPS, mainly in damage-tolerant C_f /SiC or SiC_f /SiC ceramic matrix composites or as a ceramic coating [1, 2]. However, these materials have a high Young's modulus and do not deform easily. Therefore, dedicated geometries need to be developed to ensure SiC can be considered for morphing structures. These geometries cannot be fabricated via traditional ceramic manufacturing techniques, like die pressing or injection moulding. Additive manufacturing (AM) techniques, on the other hand, do have the potential to create these complex geometries. In this study, Laser Powder Bed Fusion (LPBF) [3] was used to produce reaction-bonded silicon carbide (RBSC) components for research into morphing structures.

RBSC (also denoted as Si-SiC) is a ceramic composite material consisting of SiC, residual Si, and possibly residual C. It is conventionally produced by means of a powder metallurgy (PM) process. A porous preform consisting of SiC, C, and possibly Si is first shaped from a powder feedstock, and then infiltrated with liquid silicon at high temperatures (> 1410 °C) [4, 5]. The liquid Si infiltrates the pores of the preform due to capillary forces. In addition, it reacts with any carbon present in the preform, to produce in-situ reaction-formed SiC:

Si (I) + C (s)
$$\rightarrow$$
 SiC (s)

The resulting material is a dense RBSC, containing starting SiC, reaction-formed SiC and residual unreacted Si and C. Several studies have shown that LPBF can be used successfully in combination with carbon and silicon infiltration to obtain fully dense RBSC [6, 7].

This study aims to use LPBF of RBSC for the production of morphable control surfaces. At the same time, multi-material concepts were considered for this application and initial trials were carried out with a mix of silicon carbide and titanium. The successfully obtained materials were mechanically characterized by means of 3-point flexural testing. In addition, the thermal conductivity was measured by laser flash analysis. These results were used as input for the design of different components for morphing testing. Several "hot demonstrator" components were designed to be tested in a re-entry representative plasma environment at the von Karman Institute (VKI). These demonstrator components proved to be difficult to fabricate via LPBF, as the large structures require longer scanning times and therefore increase thermal (laser) energy input. This resulted in significant thermal residual stresses and the tendency of large cross-sections to warp in-process. This study therefore also looked at LPBF parameter and scan strategy optimisation to reduce the thermal stresses and associated warping.

Page | 2 S. Meyers, W. Declercq, J. Vleugels, B. Van Hooreweder, S. Paris, S. Débaisieux, M. Wouters, A. François, E. Kuçi, A. Parmentier, J. Steelant

2. Material Concepts

2.1. Standard RBSC

The porous preform, required to obtain RBSC by subsequent carbon and silicon infiltration, can be produced by a variety of shaping techniques. Traditional shaping techniques, like uniaxial pressing or injection moulding, all have their advantages and disadvantages. Uniaxial pressing is suitable for simple, axisymmetric shapes, whereas injection moulding is capable of producing more complex components, but is only economical for large production volumes, which are typically not encountered in the space industry. Among the more unconventional shaping techniques, AM processes have the potential to provide unlimited design freedom and short design-to-final-product cycles. On top of that, AM is also economically viable for prototypes, unique (single) components, and low production volumes. Within the MIMOSA project, laser powder bed fusion (LPBF) additive manufacturing was explored to produce materials for high-temperature morphing structures, e.g. for control surfaces for atmospheric re-entry. RBSC was the first material considered, and although it has its limitations with respect to high-temperature performance due to the presence of residual Si that melts at 1420°C, it still has the potential to be a viable material for aerospace control surfaces.

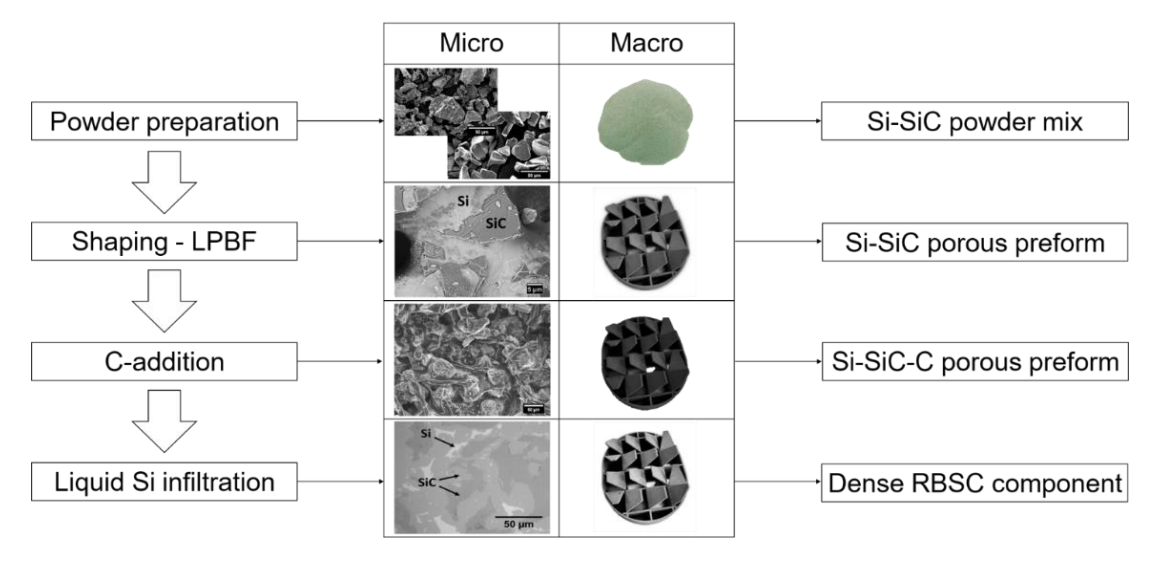


Fig. 1: PM process for the production of standard RBSC.

The process used at KU Leuven for the production of RBSC materials via LPBF is schematically shown in Fig. 1. It is a powder metallurgy process that consists of four steps. The first step is powder preparation. Silicon (Si, Nanoval, $d_{50}=26.2~\mu m$) and silicon carbide (SiC, Washington Mills, $d_{50}=29.2~\mu m$) powders were homogeneously dry mixed in a 40:60 volume ratio. This was done in a polyethylene container on a multi-directional mixer at 75 rpm for 5 hours. In the second step, the obtained powder mix was shaped using LPBF AM on a 3D Systems ProX 320 machine equipped with a 500 W continuous wave fibre laser with a spot size $(1/e^2)$ of 90 μ m and a wavelength of 1070 nm. During LPBF, thin layers of powder were spread on a build platform and selectively scanned with a laser. The consolidation mechanism consists of melting and re-solidification of the silicon, which acted as a metal binder to fuse the silicon carbide particles into a porous preform (45 vol% porosity) containing both Si and SiC. The LPBF parameters used in this work are summarized in Table 1. LPBF was performed in an inert Ar atmosphere (< 25 ppm O_2), and continuous zig-zag scanning was used with a 67° rotation between layers. Parts were pre-processed using 3D Expert software (Oqton, Germany).

Table 1. LPBF parameters for the shaping of Si-SiC powder mixtures.

P [W]	v [mm/s]	h [µm]	l [µm]
50	800	100	30

HiSST-2025-#241 Page | 3
Fabrication of Reaction Bonded Silicon Carbide Components for Morphing Control Surfaces via Laser Powder Bed Fusion 3DPrinting: Challenges and Future Perspectives Copyright © 2025 by author(s)

The third step consists of carbon infiltration into the porous Si-SiC preform. This was done via a phenolic resin, which was first loaded into the preform, and subsequently cured and pyrolysed at elevated temperatures, yielding a large amount of residual carbon (Polymer Infiltration & Pyrolysis or PIP). The resin was based on 15 ml Formalin (a 37 wt% formaldehyde solution in water), 6.25 g phenol (Acros Organics, 99%+) and 4.8 g 2-naphthol (Acros Organics, 99%+). These constituents were mixed at 700 rpm on a hot plate equipped with a magnetic stirring bar, and kept at temperatures in excess of 42°C in order to fully dissolve the 2-naphthol, until a homogeneous solution was obtained. Then, the solution was mixed with a 3M NaOH aqueous solution in a 5:1 volume ratio. The obtained polymer resin was infiltrated in the porous Si-SiC parts by vacuum or manual titration. The infiltrated components were subjected to a heat treatment in a tube furnace in N_2 atmosphere for crosslinking and pyrolysis. The heating cycle is reported in Table 2, with a natural furnace cooling down to room temperature. A total of 2 subsequent PIP cycles were performed before moving on to the final densification step.

Table 2. Thermal cycle for polymer infiltration and pyrolysis (PIP).

Ramp 1	Hold T	Hold t	Ramp 2	Hold T	Hold t
[°C/min]	[°C]	[h]	[°C/min]	[°C]	[h]
5	150	3	5	700	2

The C-Si-SiC preforms obtained after LPBF and PIP were densified by infiltration with liquid Si at temperatures in excess of 1450°C (Liquid Silicon Infiltration or LSI). The Si-SiC-C samples were placed in a graphite crucible lined with boron nitride (BN). The BN was used to avoid liquid Si from infiltrating the graphite crucible (Si has a large wetting angle on BN, but readily wets and infiltrates graphite). A certain amount of Si metal chunks was used as a source for infiltration, equal to 50% of the volume of the component to be infiltrated. LSI was performed in a graphite vacuum furnace (W100/150-2200-50 LAX, FCT Systeme) at 40 mbar following the thermal cycle presented in Table 3. The samples were naturally cooled to room temperature. During LSI, most of the infiltrated silicon reacted with the added carbon to a reaction-formed SiC, and densified the preforms. This resulted in fully dense reaction-bonded silicon carbides with increased SiC fractions. In addition, since liquid metal infiltration was used instead of solid state sintering, shrinkage was effectively avoided, and the process can be deemed a net-shaping process, i.e. the printed shape is also the final shape.

Table 3. Thermal cycle for liquid silicon infiltration (LSI).

Ramp 1	Hold T	Hold t	Ramp 2	Hold T	Hold t
[°C/min]	[°C]	[min]	[°C/min]	[°C]	[min]
40	1050	1	10	1500	30

The obtained RBSC was evaluated by optical microscopy (VHX-6000, Keyence) of polished samples. A typical cross-section is shown in Fig. 2, revealing a fully dense material consisting of 38 vol% Si (light grey), 48-54 vol% SiC (medium gray), and 8-14 vol% residual C (dark grey).

Mechanical testing was performed by 3-point bending (ElectroPuls E10000, Instron) on bar-shaped samples (3x4x45 mm³). These samples were prepared as per ASTM C1161-13, and were finished by planar grinding. A total of 27 samples were tested, and the results were analysed via Weibull statistics. They are visually presented in Fig. 3, where the probability of survival is plotted versus the flexural strength. This data set allowed to assess the Weibull modulus and characteristic strength.

HiSST-2025-#241 Page | 4 S. Meyers, W. Declerco, J. Vleugels, B. Van Hooreweder, S. Paris, S. Débaisieux, M. Wouters, A. François, F. Kuci, A.

Copyright © 2025 by author(s)

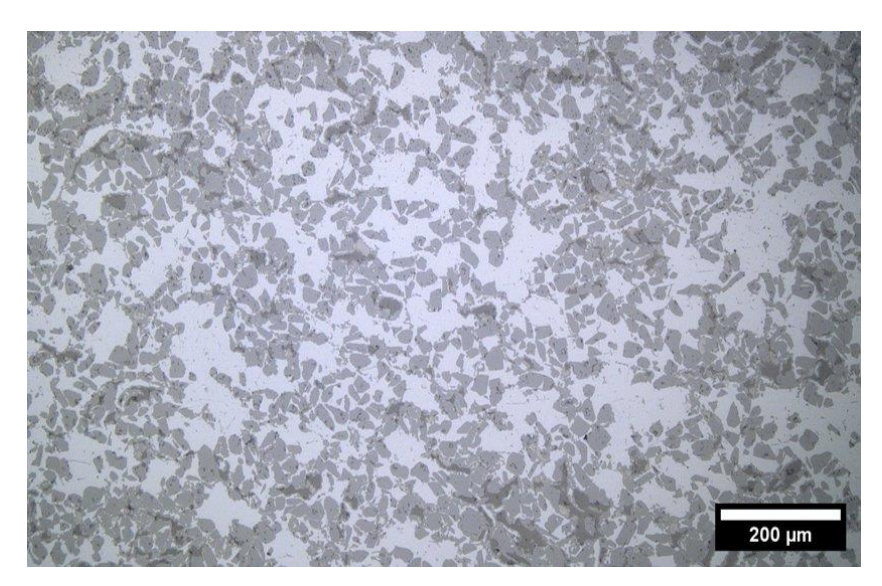


Fig. 2: Optical micrographs of a typical RBSC obtained by powder mixing, LPBF, 2x PIP and LSI resulting in a fully dense material. Three distinct phases can be observed, i.e. Si (bright), SiC (grey) and C (dark).

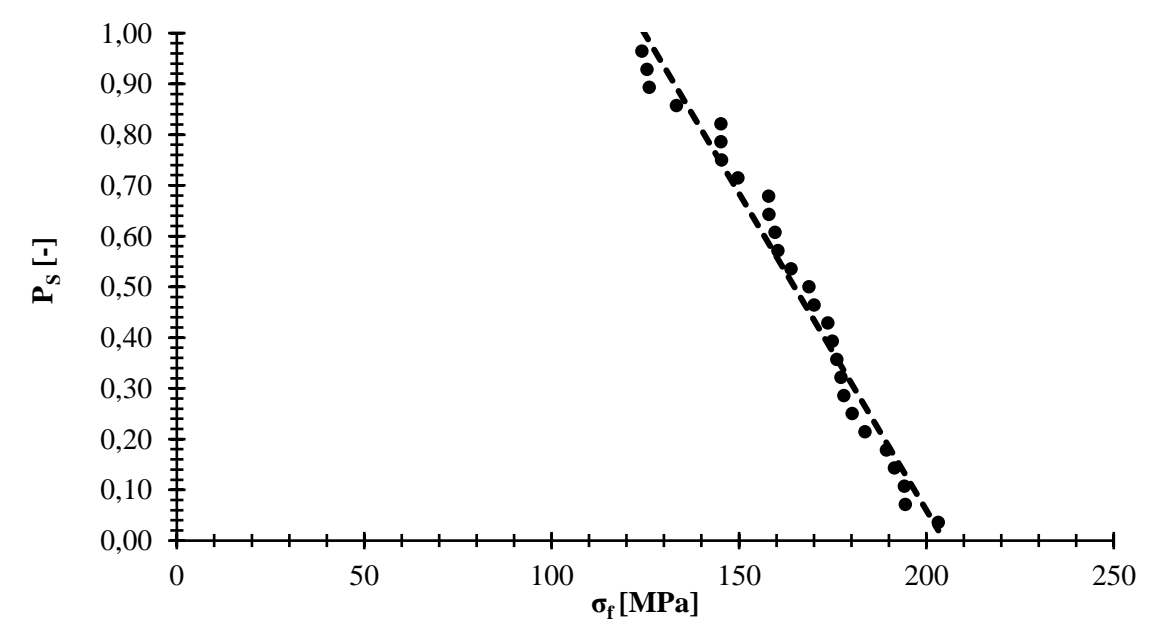


Fig. 3: Probability of survival (y-axis) versus 3-point flexural stress for 27 RBSC samples.

Along with flexural strength testing, the Young's modulus was assessed non-destructively via the Impulse Excitation Technique (IET, Grindosonic MK7) according to ASTM Standard C1259-94. Measurements were carried out at room temperature and subsequently at increasing temperatures up to 1000 K. The measured mechanical properties are summarized in Table 4. The following observations can be made:

- The Weibull modulus m is 7.9. The higher this value, the steeper the probability of survival versus strength plot, and the higher the quality of the production process (less variability on the produced samples). Typically for technical ceramics, the aim is to reach an m > 10.
- The elongation at break is very low, ~0.1%, which is typical for ceramic materials. This conflicts with the morphing requirement.
- The Young's modulus decreases with temperature, but very mildly.

Table 4. Mechanical properties of the standard RBSC derived from IET and 3-point bending tests and Weibull analysis on 27 RBSC samples.

σ _{flex} [MPa]	σ _{char} [MPa]	m [-]	ε [%]	E _{T = 278K} [GPa]	E _{T = 1000} к [GPa]
165 ± 22	175	7.9	0.098	221	212

2.2. Optimised RBSC

A new process methodology was established with the objective of improving the SiC content and the final properties of the Si-SiC material discussed in section 2.1. The newly designed process methodology consisted of six steps rather than four and is schematically shown in Fig. 4. The steps in this process are the same as previously stated, and are performed with the same set of parameters. However, after the first two PIP cycles, an intermediate SiC conversion step is added, after which PIP is repeated a number of times before performing LSI.

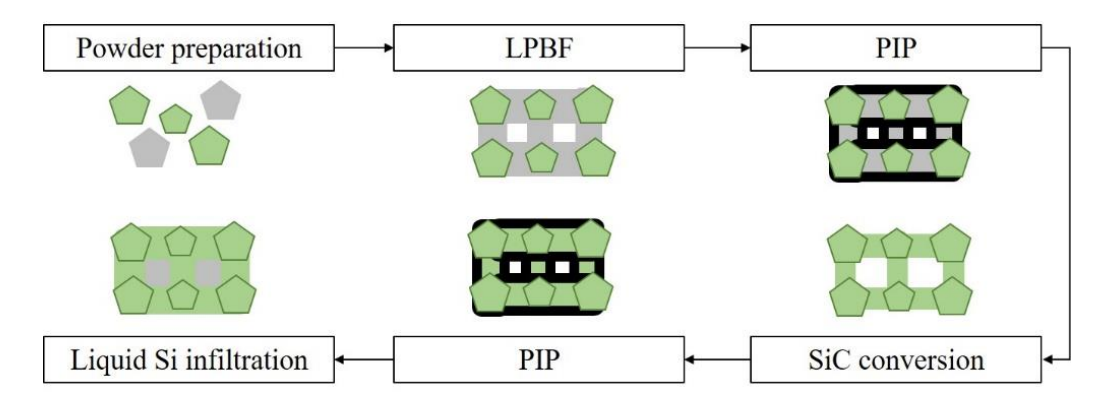


Fig. 4: Updated process methodology for the production of optimised Si-SiC via LPBF.

The SiC conversion step is performed with the aim of converting the Si used in the powder mix during LPBF into SiC. This is done via a high-temperature heat treatment using the parameters specified in Table 3 (identical to LSI). During SiC conversion, the Si in the preform can react with the C added during PIP, in order to fully convert into SiC.

In order to determine the optimal amount of PIP cycles after SiC conversion, samples were produced with 1, 2, 3, and 4 PIP cycles, before being densified by LSI. These RBSCs were analysed by optical microscopy and image analysis software (ImageJ) in order to assess the amount of Si, SiC, C, and residual porosity. The microstructures are presented in Fig. 5. The following observations can be made:

- RBSCs subjected to 1 and 2 PIP cycles are fully dense.
- RBSCs subjected to 3 and 4 PIP cycles show considerable porosity of 3 and 16 vol%, respectively. This porosity is likely caused by pore choking owing to the volume expansion taking place when Si reacts with C. The newly formed SiC blocks the pore channels, inhibiting complete capillary infiltration of Si.
- The RBSC subjected to 2 PIP cycles was measured to have the highest SiC and lowest residual Si content. The final material composition was 62 vol% SiC (versus 48-54 vol% in the standard RBSC), 28 vol% Si (versus 38 vol% in the standard RBSC), and 10 vol% C (versus 8-14 vol% in the standard RBSC).

HiSST-2025-#241

Page | 6

S. Meyers, W. Declerco, J. Vleugels, B. Van Hooreweder, S. Paris, S. Débaisieux, M. Wouters, A. François, F. Kuci, A.

Copyright © 2025 by author(s)

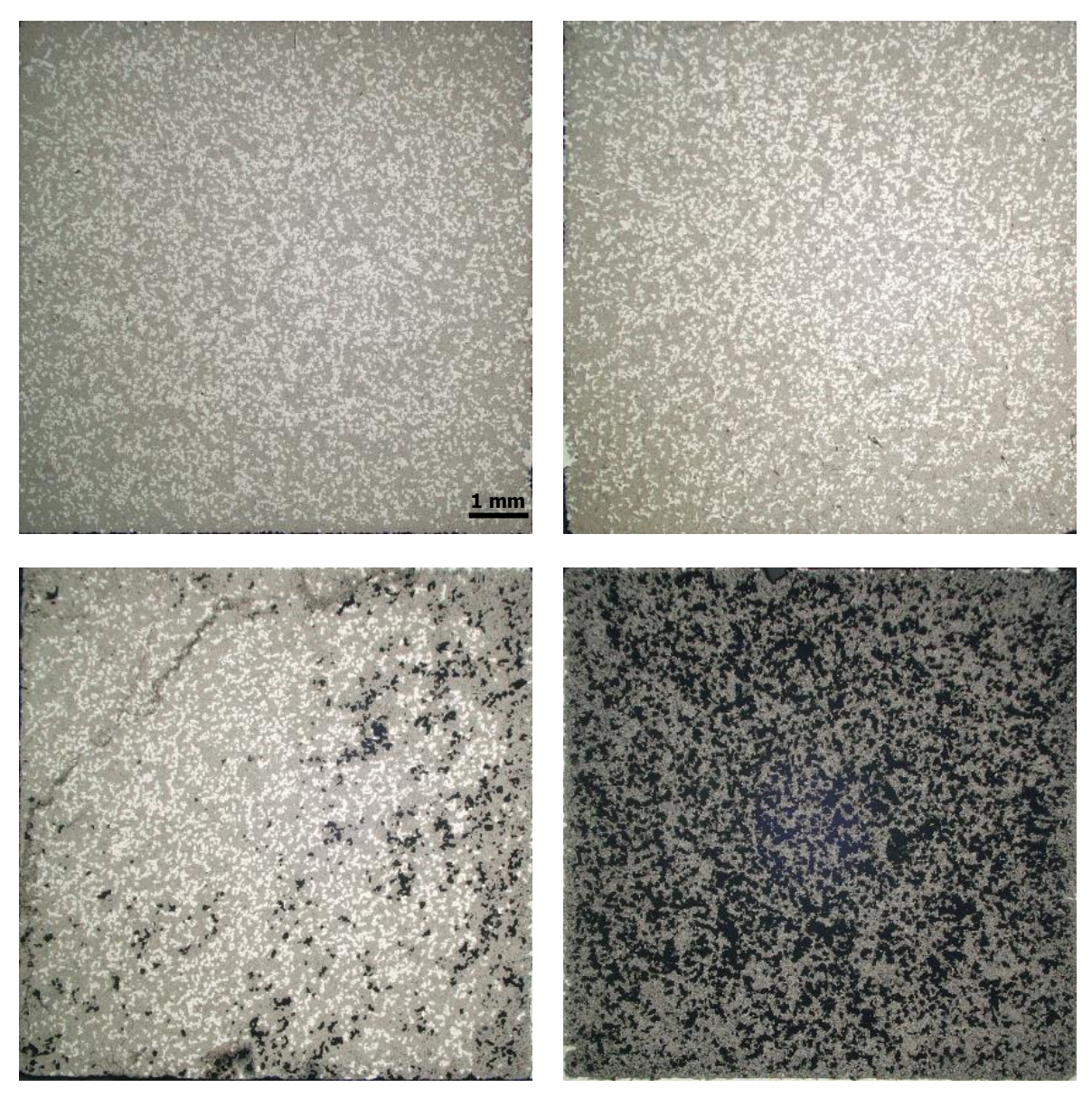


Fig. 5: Optical microscopy images of RBSC with 1 (top left), 2 (top right), 3 (bottom left) and 4 (bottom right) PIP cycles after intermediate SiC conversion.

The optimal production cycle therefore consists of powder preparation, LPBF, 2x PIP, SiC conversion, 2x PIP, and LSI. This methodology was used to produce 9 test specimens for 3-point bending mechanical testing according to ASTM C1161-13. The results are summarised in Table 5.

The thermal conductivity of 136 W/mK at room temperature reduced to 74 W/mK at 300°C, as measured by laser flash analysis (LFA 467, HyperFlash).

Table 5. Mechanical and physical properties of the optimised RBSC derived from IET, laser flash, and 3-point bending tests on 9 RBSC samples.

σ _{flex}	ε	E	k	ρ
[MPa]	[%]	[GPa]	[W/mK]	[g/cm³]
221 ± 21	0.10 ± 0.011	266 ± 5	136	2.8

Some concluding remarks should be made on the RBSC material, keeping in mind its potential for morphing structures:

- The optimised production cycle resulted in a material with a higher SiC content, and consequently better mechanical properties, with a flexural strength up to 221 MPa and Young's Modulus of 266 GPa.
- The elongation at break however remains limited to 0.1%, typical for a technical ceramic. This limits the morphing potential of the material immensely. In order to obtain a truly morphable ceramic-layer containing based flap design, other solutions will have to be envisaged.

2.3. Multi-Material Concepts

In order to fulfil the requirements specified in the project, especially with respect to deformability, a multi-material was envisaged combining the heat/harsh environment resistance of RBSC with the ductility and damage tolerance of a metal, in this case Ti6Al4V, a material that is well known to be suitable for production via LPBF. The initial concept consisted of:

- RBSC, 3D printed on the hot side, subjected to the re-entry gas flow. In the morphed state, the ceramic would be largely loaded in compression;
- Ti6Al4V (Ti64), 3D printed on the cold side, to add morphing capability by ductility, and to provide a damage-tolerant backing layer for the RBSC. In addition, structures and features can be foreseen to facilitate integration of the morphable flap with the spacecraft's main structure (lugs, attachment points, lattices).

Different strategies were investigated in order to combine these two materials.

2.3.1 Printing of Ti64 on RBSC

A Si-SiC plate (50x50x2 mm³) was printed on an Mlab Cusing R LPBF machine (Colibrium Additive, formerly Concept Laser GmbH) with a laser power of 15 W, a scanning speed of 100 mm/s, a hatch spacing of 77 µm and a layer thickness of 30 µm. The Mlab is equipped with a 100 W continuous wave fibre laser with a spot size (1/e²) of 50 µm and a wavelength of 1070 nm. The process was carried out in inert Ar atmosphere (<0.3% O₂) using continuous zig-zag scanning with a 90° rotation between layers. Subsequently, different Ti64 cylinders were printed on top of the porous Si-SiC substrate in the same LPBF machine. For the binding layers (the first five layers), a variety of LPBF parameters were applied, with laser powers varying from 45 to 95 W and scanning speeds from 300 to 900 mm/s, with a fixed layer thickness of 30 µm and a hatch spacing of 77 µm. The subsequent layers were built with nominal parameters (P = 45 W, v = 600 mm/s, h = 77 μ m and l = 30 μ m). The results are shown in Fig. 6. As can be observed, the majority of the cylinders failed due to warping of the scanned layers, resulting in single layers detaching from the Si-SiC plate during building, making it impossible to produce a 3D titanium part. However, two of the cylinders were moderately successful. The first five layers of these cylinders were produced with a power of 95 W and a scanning speed of 300 mm/s, whilst the subsequent layers were scanned with nominal parameters of 45 W and 600 mm/s. When taking a closer look at these cylinders, however, a brittle interface can be observed, and the Ti cylinder easily detached from the Si-SiC.

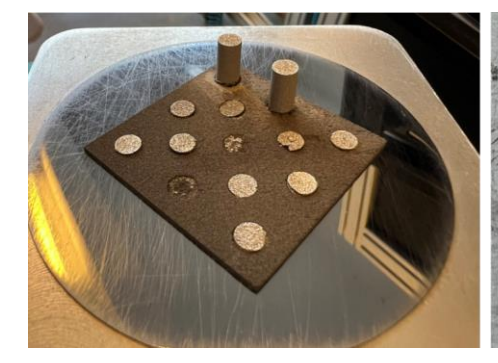




Fig. 6: Ti64 printed on top of a porous printed Si-SiC substrate.

It is clear that this strategy is severely limited because the excessive heat input during Ti printing cannot be conducted away from the scanned layers, since the Si-SiC substrate is porous and therefore has a very low thermal conductivity. This results in thermal stress build-up and warping of the Ti layers during the LPBF process. Printing Ti64 on top of a dense RBSC substrate, however, should alleviate some of these issues, and was therefore attempted next.

A dense RBSC cube was used as substrate to coat and laser scan titanium. The resulting structure is shown in Fig. 7. The Titanium was scanned with a variety of parameters, before settling on a laser power of 50 W and a scanning speed of 444 mm/s. Two observations can be made:

- In-process warping still occurs. The Ti detached from the RBSC substrate;
- The dense RBSC substrate seems to be eroded away at the relatively higher laser powers used to scan the Ti (50 W versus the nominal 15 W for Si-SiC).

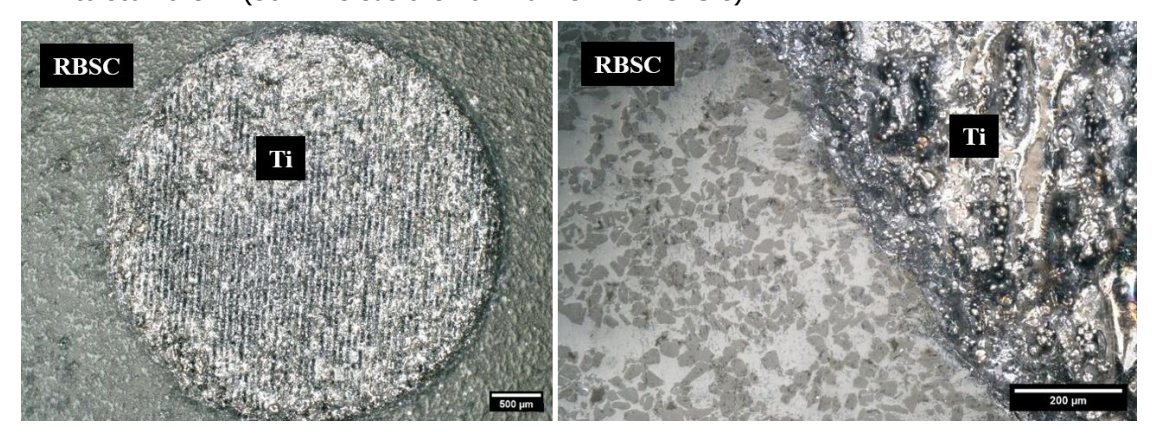


Fig. 7: Top view of Ti layers printed on top of a dense RBSC cube.

In order to alleviate the issue with laser erosion, the Ti was subsequently scanned with a lower laser power of 15 W and a scanning speed of 100 mm/s. This had a beneficial effect, and the Si-SiC was no longer eroded away. However, in-process warping still occurred, resulting in detachment of the scanned Ti layers from the SiC substrate. The warping is likely caused by the difference in thermal expansion coefficient (CTE) between Ti and Si-SiC. Ti has a CTE of $8.5 \times 10^{-6} \, (^{\circ}\text{C}^{-1})$ and Si-SiC has a CTE which is less than half that value, i.e. 2.7- $4.3 \times 10^{-6} \, (^{\circ}\text{C}^{-1})$. In conclusion, printing of Ti64 on top of RBSC was shown to be challenging and warping always occurs. The mismatch in CTE between Ti64 and Si-SiC is a technical bottleneck.

2.3.2 Printing of Si-SiC on Ti64

A preliminary proof-of-concept test was performed, where Si-SiC was laser scanned on top of dense, LPBF Ti cuboid substrates. The Si-SiC was scanned with a variety of laser powers and scanning speeds, resulting in four successful samples, all scanned with the nominal parameters used for Si-SiC, i.e. a laser power of 15 W and a scanning speed of 100 mm/s. Based on these encouraging results, larger components were printed: two 30 x 30 mm 2 Ti64 lattice structures with backing plates were subsequently used as substrates for Si-SiC recoating and laser scanning. A 1 mm Si-SiC plate was fabricated via LPBF on top of these Ti64 substrates. The result after hybrid LPBF is shown in Fig. 8. Visually, a good connection between the Ti and the Si-SiC can be observed without in-process warping.

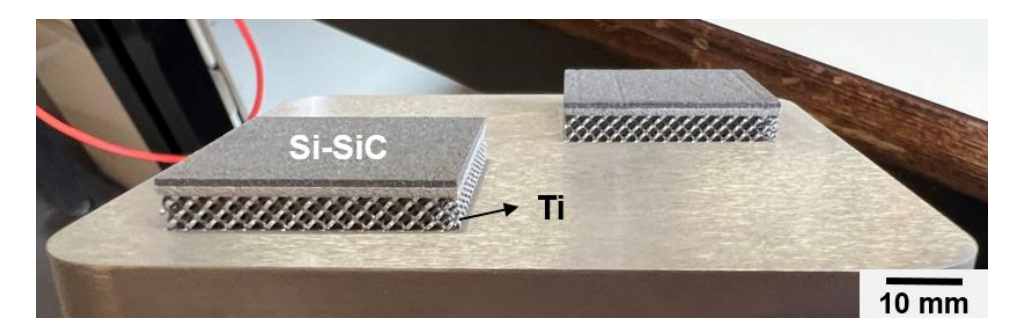


Fig. 8: LPBF Si-SiC plate with a thickness of 1 mm built on top of a LPBF Ti64 diamond lattice with a dense intermediate backing plate. The footprint area of the components is $30 \times 30 \text{ mm}^2$.

The Si-SiC still has to be densified after printing. In order to achieve this, the "conventional" densification route of PIP and LSI was avoided due to the high possibility of creating brittle Ti-Si interfaces as well as the required temperatures which are necessary for the LSI process (1450-1500°C). Instead, a preceramic poly-siloxane resin was used in a multiple PIP cycle approach. The poly-siloxane pyrolysis forms an amorphous SiOC ceramic phase. The heating cycle is presented in Table 6, and was conducted in inert Ar atmosphere. The PIP was repeated for a total of 5 cycles. The complete, new powder metallurgy process, which omits C- and liquid Si infiltration, is presented in Fig. 9.

Table 6. Thermal cycle for preceramic polymer resin PIP.

Ramp 1	Hold T	Hold t	Ramp 2	Hold T	Hold t
[°C/min]	[°C]	[min]	[°C/min]	[°C]	[min]
2	300	30	5	1000	120

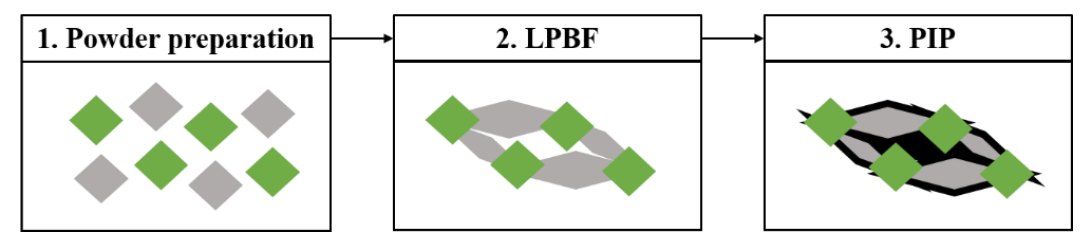


Fig. 9: 3-Step PM process for densification of Si-SiC by preceramic polymer (i.e. a poly-siloxane Si-O-C precursor) PIP (up to 5 times). Si: light grey, SiC: green, Si-O-C: black.

After the 5 PIP cycles, the sample was embedded and polished in order to reveal the microstructure of the obtained material. The cross-section shown in Fig. 10, with Ti on the bottom and Si-SiOC-SiC on top, reveals no significant defects or cracks at the interface. However, the Si-SiOC-SiC material is not fully dense, since porosity can be clearly identified as the black phase.

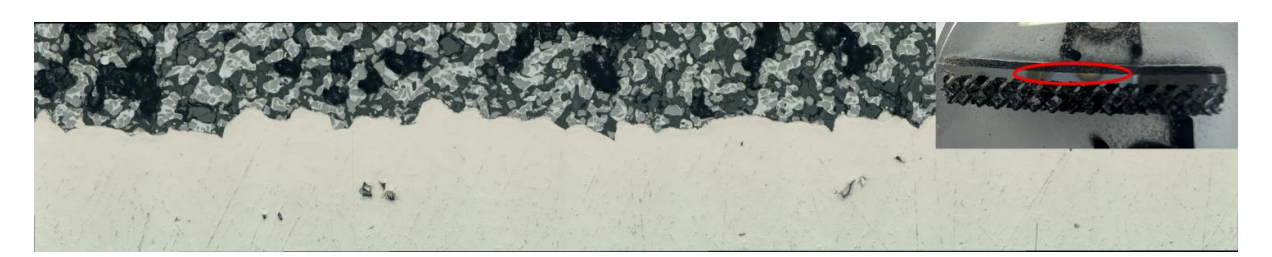
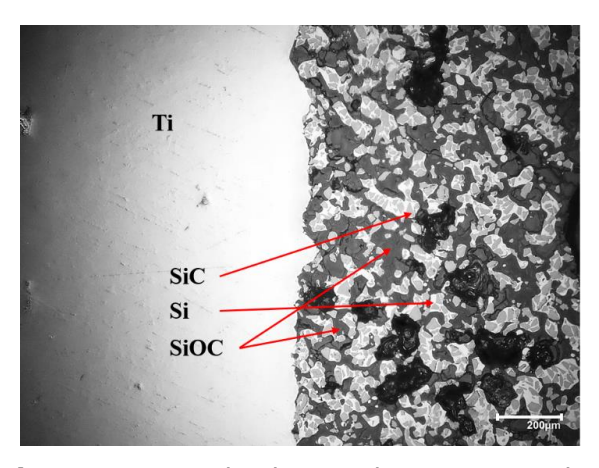


Fig. 10: Cross-section of the interface of a hybrid material component (top: Si-SiOC-SiC, bottom: Ti). The component is presented in the top right corner of the figure, with the red circled area representing the area shown on the micrograph.

The interface of this hybrid material was studied at higher magnifications, as presented in Fig. 11, revealing a clearer view on the porosity, the different phases and the interface between Ti and Si-SiOC-SiC, which seems to be a different phase (different color) than the Ti, and possibly consists of a Ti-Si.

HiSST-2025-#241 Page | 10 S. Meyers, W. Declerco, J. Vleugels, B. Van Hooreweder, S. Paris, S. Débaisieux, M. Wouters, A. François, F. Kuci, A.

Copyright © 2025 by author(s)



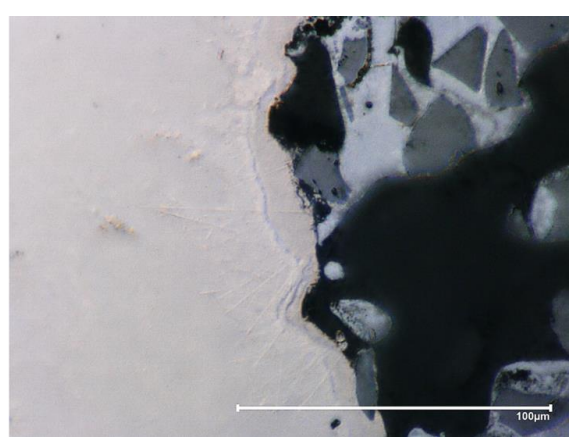
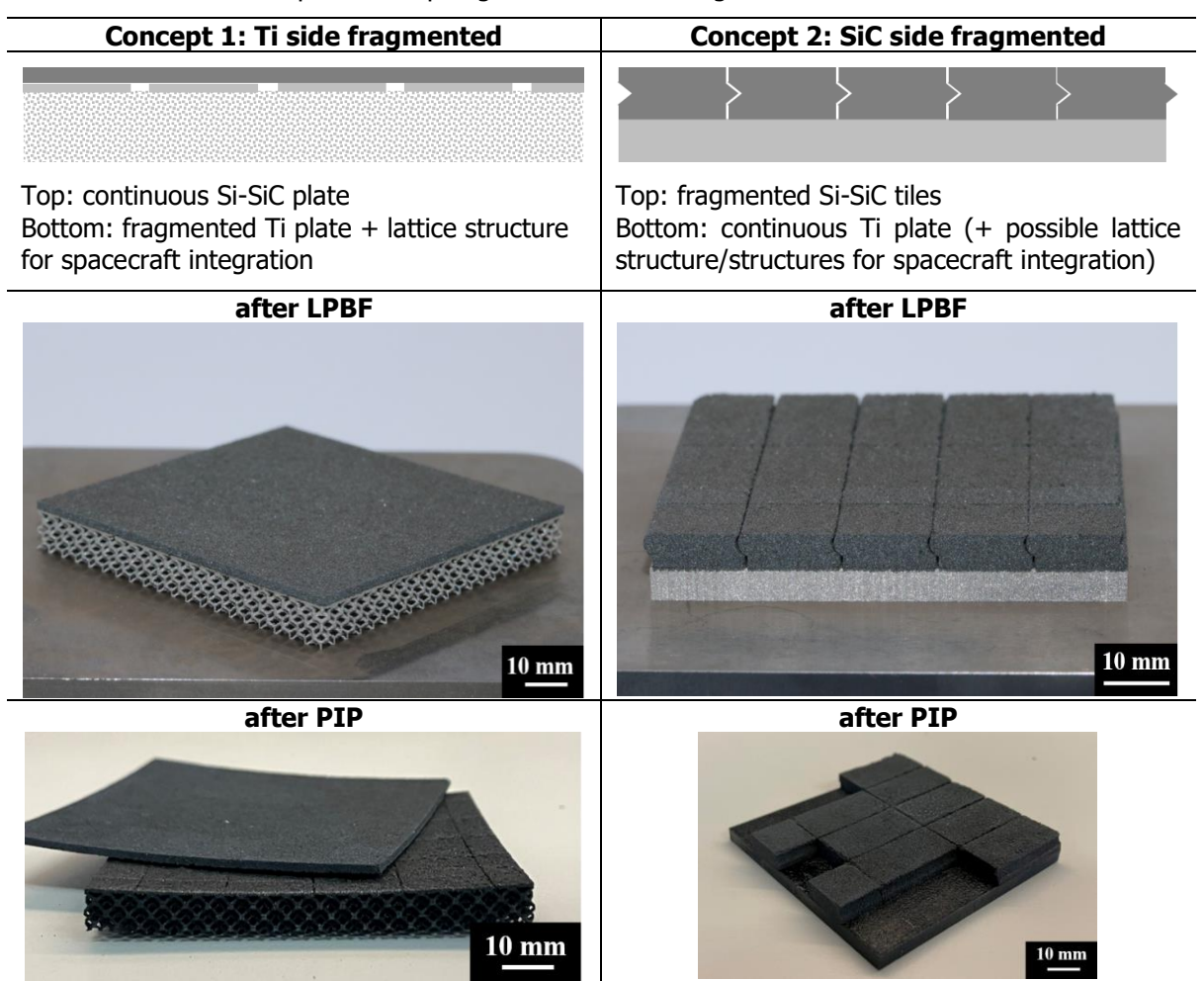


Fig. 11: Micrographs showing the constituent phases present in the hybrid material (left), as well as the interface between Ti and Si-SiOC-SiC (right).

Upscaling to larger footprint geometries and larger components was a necessity to reach the objectives of the MIMOSA project, so a new test campaign was run with larger components. However, a footprint of $50 \times 50 \text{ mm}^2$, even after successful building via LPBF, failed during the PIP furnace cycles. The identified cause was the difference in CTE between Ti and the ceramic material, resulting in thermal stress generation during heat treatment, especially for larger components. In order to mitigate this, different concepts were conceived in which the contact area between the printed Si-SiC and Ti was fragmented to minimise the effect of the CTE mismatch. These concepts are presented in Table 7.

Table 7: Different concepts for morphing structures with fragmented interface between Ti and Si-SiC.



The concepts presented above were printed as 50x50 mm² footprint components, as shown in the pictures in Table 7. After printing, both concept components were subjected to PIP with a SiOC precursor resin according to the PM process presented in Fig. 9. The final result is shown in the bottom row of Table 7:

- For concept 1, detachment of the top Si-SiOC-SiC layer took place in the second PIP cycle. As the Si-SiOC-SiC material is densified, it becomes more rigid and therefore cannot compensate for the difference in CTE with Ti during cooling.
- For concept 2, detachment of some tiles occurred during electrical discharge machining of the part from the titanium base plate. Afterwards, several PIP cycles were completed, resulting in even more tiles detaching from the Ti bottom plate.

As a conclusion to the multi-material concepts, it is clear that the mismatch in CTE between the ceramic material and Ti64 causes a variety of issues, not only during printing, but also and especially during thermal post-treatments.

3. Final Material Selection

For the application of an aerodynamic control surface (flap) for a re-entry vehicle, the only material that has the maturity and therefore potential candidate is the optimised standard RBSC, described in section 2.2. The properties of this material were summarised in Table 5. Regrettably, the hybrid material options, whilst promising on paper, require more dedicated research to achieve a higher TRL. The standard RBSC material has its own drawbacks, namely, low deformability and toughness, evidenced by the low elongation at break. However, it is expected that the material is more morphable at temperatures in excess of the ductile-to-brittle transition temperature of silicon, which is typically between 540-550°C [8].

4. Demonstrator Fabrication

In order to fabricate the hot demonstrators for Plasmatron testing at VKI, different LPBF scan strategies were explored. Since the demonstrators consist of a flat plane measuring 80x90 mm², the cross-sectional area to be scanned in the first layers is rather large and prone to developing thermal stresses. The first layers were therefore scanned with an island scan strategy. The cross-section is divided into small 10x10 mm² 'islands', which are scanned in order. In this way, long scan vectors are avoided. In addition, the island size is the same as the size of the small cubes that were used to obtain the optimal process parameters, implying that the parameters should translate well to these larger structures. A schematic view of an island scanning strategy is shown on the left in Fig. 12.

For the fin hot demonstrators, the layers following the large plane area were scanned normally, i.e. continuously. For the pillars, however, a multi-contour scan strategy was employed, whereby each pillar is scanned by means of subsequent concentric circles. A schematic representation of the multi-contour scan strategy can be seen in Fig. 12.

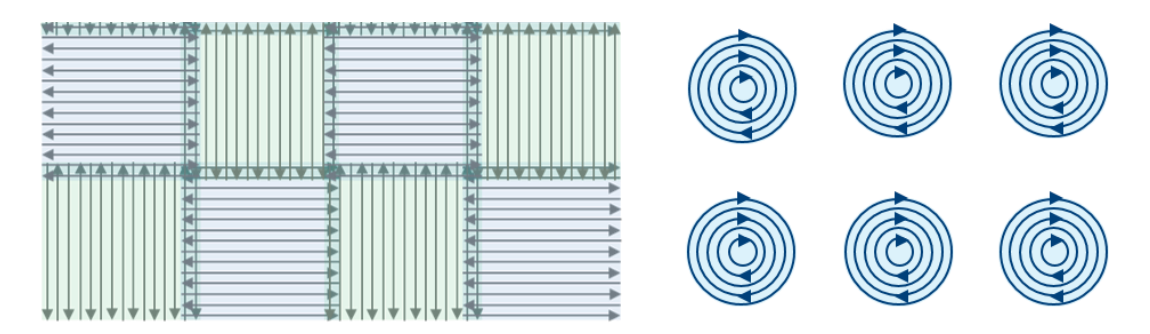


Fig. 12: Schematic representation of an island scan strategy (left) used for the fin concept and a multi-contour scan strategy (right) used for the pillar concept, where arrows represent the scan vectors, i.e. the path the laser follows during processing.

Despite the use of island scanning for large cross sections, in-process warping due to thermal stresses remained an issue. Both warping of the silicon wafer baseplate itself as well as the scanned component were observed. This resulted in a failure rate of around 50%. Failure typically occurred within the first 20 layers. Despite this, 7 hot demonstrator components were successfully fabricated, 3 of which were blade stiffener hot demonstrators, and 4 were pillar stiffener hot demonstrators. Some of these are shown in Fig. 13. In addition, two Ti6Al4V hot demonstrators were fabricated to verify the test set-up.



Fig. 13: Collection of hot demonstrator components: Ti dummy plate (left), blade stiffener Si-SiC hot demo (middle), and pillar stiffener Si-SiC hot demo (right).

After LPBF printing and post-processing, dense RBSC hot demonstrator components were obtained. A finished pillar stiffener hot demonstrator is presented in Fig. 14. All of the finished hot demonstrators were measured with a tactile measurement device, and one of them via CT scanning, in order to assess the dimensional accuracy of the production process. The tactile measurements were conducted along 10 points for plate thickness, 3 points for lug hole diameter, and 5 points for fin thickness or pillar diameter. In addition, plate curvature was measured as the vertical distance from the bottom of the clamping end of the plate to the bottom of the lug end of the plate. The measurement points are schematically shown in Fig. 15. Measurement data can be found in Table 8 and Table 9, along with the original CAD file dimensions. Clearly, further LPBF and PM process optimisation has to be carried out in order to ensure higher dimensional accuracy and reduce or eliminate warping.



Fig. 14: Finished pillar stiffener Si-SiC hot demonstrator component.

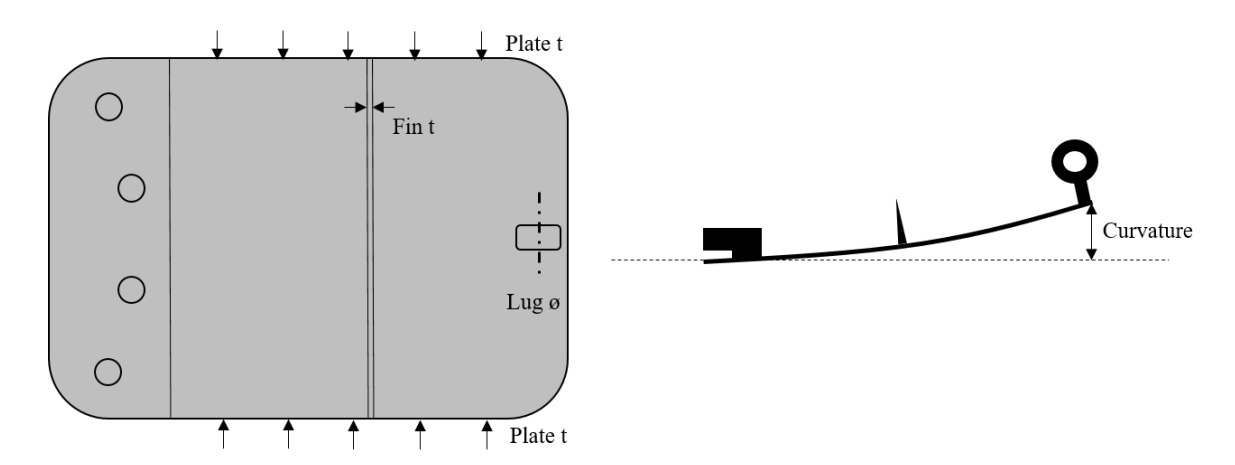


Fig. 15: Schematic view of the measurement points on the fin hot demonstrator. Measurement points on the pillar hot demonstrator are the same, with the exception of having the fin thickness replaced by the pillar diameter.

Table 10. Tactile dimensional assessment of three fin hot demonstrators, along with original CAD design dimensions.

	Plate t [mm]	Fin t [mm]	Lug hole ø [mm]	Curvature [mm]
CAD design	0.8	0.81	6	0.15
#1	1.16 ± 0.04	1.01 ± 0.02	5.96 ± 0.02	1.08//1.16//0.77
#2	1.07 ± 0.05	1.02 ± 0.02	5.88 ± 0.01	0.55//0.63//0.95
#3	1.01 ± 0.06	0.99 ± 0.01	5.96 ± 0.03	0.09//0.07//0.04

Table 11. Tactile dimensional assessment of four pillar hot demonstrators, along with original CAD design dimensions.

	Plate t [mm]	Pillar ø [mm]	Lug hole ø [mm]	Curvature [mm]
CAD design	0.7	0.9	6	0.15
#1	1.10 ± 0.04	1.02 ± 0.02	5.87 ± 0.02	0.65//0.69//0.69
#2	1.09 ± 0.04	1.01 ± 0.02	5.86 ± 0.03	0.92//0.80//1.04
#3	1.06 ± 0.03	0.99 ± 0.02	5.85 ± 0.03	1.20//1.34//1.25
#4	0.99 ± 0.03	0.97 ± 0.02	5.91 ±0.02	//

Plasmatron testing was conducted on the 7 produced hot demonstrator samples. Regrettably, only one test was successful, with the other tests failing due to sudden fracturing of the demonstrator components. The failed and successful tests are described in more detail in another submitted paper [9]. The successful test was performed on a pillar concept hot demonstrator and resulted in a rather limited maximum measured deflection of approximately 2 mm over the total length of the demonstrator, i.e. 90 mm.

5. Conclusions & Future Perspectives

The experimental work proves that reaction-bonded silicon carbide materials can be produced via laser powder bed fusion 3D-printing, allowing for the fabrication of tailored and specific designs and opening up possible advancements into the research on morphing structures. The LPBF printing strategies can be adapted to produce large components in sizes representative for relevant applications in control surfaces for re-entry vehicles.

Reaction bonded SiC is a very stiff and brittle material, and although it is an interesting candidate material for thermal protection systems, it is not an ideal material for morphing applications due to its

S. Meyers, W. Declercq, J. Vleugels, B. Van Hooreweder, S. Paris, S. Débaisieux, M. Wouters, A. François, E. Kuçi, A. Parmentier, J. Steelant

intrinsic monolithic ceramic nature. For this reason, multi-material structures combining a more ductile metal with the brittle RBSC material were explored. Initial testing showed an important bottleneck caused by the significant mismatch in CTE between metal and ceramic. Dedicated efforts are required in order to overcome the challenges encountered by that.

Acknowledgements

The authors gratefully acknowledge the funding under ESA contract no. 4000140022/22/NL/MG (Morphing of Aero-Thermally Loaded Structures). Furthermore, we would like to extend our gratitude to Wout Veulemans for assistance in preparing the ceramic samples for mechanical testing, as well as to Eddy Smets for wire EDM work.

References

- 1. Uyanna, O. & Najafi, H.: Thermal protection systems for space vehicles: a review on technology development, current challenges and future prospects. Acta Astronautica (2020).
- 2. Sutton, G. W.: The initial development of ablation heat protection: an historical perspective. J. Spacecraft Rock. (1982).
- 3. Kruth, J.-P., Levy, G., Klocke, F. & Childs, T.: Consolidation phenomena in laser and powder-bed based layered manufacturing. CIRP Annals Manufacturing Technology, 56(2), 730-759 (2007).
- 4. Ruys, A.J.: Chapter 6 Reaction Sintered SiC (RSSC). In: Ruys, A.J.: Silicon Carbide Ceramics, Ed. Elsevier, 349-394 (2023).
- 5. Sangsuwan, P., Orejas, J. A., Gatica, J.E., Tewari, S.N. & Singh, M.: Reaction-bonded silicon carbide by reactive infiltration. Industrial & Engineering Chemistry Research, 40(23), 5191-5198 (2001).
- 6. Evans, R.S., Bourell, D.L., Beaman, J.J. & Campbell, M.I.: Rapid manufacturing of silicon carbide composites. Rapid Prototyping Journal, 11, 37-40 (2005).
- 7. Stevinson, B.Y., Bourell, D.L. & Beaman, J.J.: Support-free infiltration of selective laser sintered (SLS) silicon carbide preforms. Solid Freeform Fabrication Symposium, Austin, Texas, 359-365 (2006).
- 8. Hirsch, P.B. & Roberts, S.G.: The brittle-ductile transition in silicon. Philosophical Magazine A, 64(1), 55-80 (1991).
- Paris, S., Holum, S., Débaissieux, S., Wouters, M., Fraçois, A., Parmentier, A., Meyers, S., Declercq, W. & Steelant, J.: Experimental characterization of morphing structures for space applications under thermal and mechanical load. HISST: 4th International Conference on High-Speed Vehicle Science Technology, Tours, France (2025), HiSST-2025-0227.

HiSST-2025-#241 Page | 15 Fabrication of Reaction Bonded Silicon Carbide Components for Morphing Control Surfaces via Laser Powder Bed Fusion 3D-